Ice Mass Balance and Antarctic Gravity Change: Satellite and Terrestrial Perspectives

Erik R. Ivins[1], Eric Rignot[1], Xiaoping Wu[1], Thomas S. James[2], and Gino Casassa[3]

[1] Jet Propulsion Lab, Caltech, Pasadena, USA *eri@fryxell.jpl.nasa.gov*
[2] Geological Survey of Canada, Sidney, BC, Canada
[3] Centro de Estudios Cientificos, Climate Change & Glaciol. Lab., Valdiva, Chile

Summary. Recent advances in the spatial and temporal retrieval of land-based cryospheric change information south of 42.5° allow fairly robust construction of forward model predictions of the time-rate of change in gravity. A map-view prediction is presented for the time-rate of change in geoid, $d\mathsf{N}/dt$ that might be retrieved from the currently orbiting gravity space craft, CHAMP (Challenging Mini-Satellite Payload for Geophysical Research and Application) and/or GRACE (Gravity Recovery and Climate Experiment). Complementary computation of the surface gravity change, $d\delta g/dt$, is also presented. The latter can be recovered from terrestrial absolute gravity measurements. Also, the computed rate of change Stokes coefficients for degree and order ℓ, m 1-12 may be used as reliable estimates of the Southern Hemisphere cryospheric change contribution to the global low-degree harmonic variability recorded in multidecadal satellite laser ranging (SLR) data sets.

Key words: CHAMP, GRACE, sealevel rise, cryosphere

1 Introduction

With the launching of the CHAMP and GRACE gravity satellite missions scientists are now provided with a new opportunity to decipher interannual and interdecadal hydrological changes that may have wide-sweeping societal implications about changes in the storage and replenishment of large freshwater reservoirs across the globe [1]. The Antarctic ice sheet stores a water mass having the potential to raise equivalent sealevel by 57 meters. The stability of this mass to wasting is quite sensitive to year-to-year changes in oceanic thermal structure [2]. The level of accuracy provided by the new gravity missions [3] implies that stand-alone satellite gravity data sets might be brought to bear on the question of Antarctic ice mass change. The main goal of this paper is to employ very recent estimates of ice mass balance to investigate the implications for measurement of the time-dependent gravity south of 42.5°.

2 Time-varying Stokes Coefficients

A main goal of non-tidal time-varying gravity field determination is to isolate perturbations to the external gravitational potential on a rigid Earth:

$$\mathcal{T}(r,\theta,\lambda,t) \;=\; \frac{GM}{r}\;\sum_{\ell=1}^{L}\sum_{m=0}^{\ell}\sum_{j=1}^{2}\{\frac{R_e}{r}\}^{\ell}\;\dot{\bar{C}}_{\ell mj}(t)\;\bar{Y}_{\ell mj}(\theta,\lambda) \qquad (1)$$

where r, θ, λ, t are radial position, colatitude, longitude and time, respectively, and GM is the product of the universal gravitational constant and planetary mass. The Earth's surface gravity is g, and mean radius, R_e. Here $\bar{Y}_{\ell mj}$ are normalized real surface harmonics [4] and $\bar{C}_{\ell mj}$ are the Stokes coefficients with the symbol $\{\dot{}\}$ for time differentiation. We call these later parameters the time-varying Stokes coefficients and consider physics in which these are primarily driven by surface density changes $\dot{\sigma}(\theta,\lambda,t)$ at $r = R_e$. Variations that conserve mass allow the sum (1) to begin at $\ell = 1$.

2.1 The 27-year Record from the Lageos Class SLR Measurements

Since the launch of Starlette and Lageos I in the mid-1970's continuous monitoring of $\dot{\bar{C}}_{\ell 01}$ for $\ell = 2, 3, 4, 5, 6, 7$ has been maintained. Since about 1992, when a constellation of similar small passive satellites were in orbit, these have been increasingly reliable observations. There are mass balance coefficient relations that link these observations to total nonsteric sealevel change [4] [5] [6]. However, there exists a large number of poorly modeled sources, aside from glacial isostatic adjustment (GIA) which drives a large component of the secular part of the signal [5]. A main inference derived from the even and odd-chained secular zonal signal, after correcting for GIA, is that Antarctica may be contributing to equivalent nonsteric sealevel rise rate (ESLRR) of about $\dot{\xi}_A$ = -0.05 to +0.6 mm/yr [5] [6], but with a number of critical caveats and rather indeterminable error estimates. The situation for Antarctica, however, has now taken a turn for the better as we now discuss.

2.2 12-year Record of Mass Balance Monitoring

Radar and laser altimetry, on-ice GPS, speckle tracking of ice flow by remote sensing, ocean temperature and salinity measurements, passive microwave monitoring from space, ice core data, and grounding line migrations determined from InSAR, now provide a wealth of new data from which the mass balance of the principal ice drainage basins of Antarctica may be obtained [7]. In some parts of East Antarctica the formal errors are comparable to the drainage basin imbalance estimate. However, these form a relatively small portion of the total, and are sufficiently small in amplitude that they do

Table 1. Model ESLRR (equivalent sealevel rise rates) in mm/yr.

$\dot{\xi}_A$	$\dot{\xi}_{NZ}$	$\dot{\xi}_{SSA}$	$\dot{\xi}_{AP}$
0.2410	0.0002	0.1050	0.0809

not degrade a quantitative estimation of satellite retrieved gravity changes south of the Antarctic Circle. With new Shuttle Radar Topography Mission (SRTM) data now available for elevation control, revised estimates for the Northern and Southern Patagonian icefields show that the ice mass loss to the oceans during the period 1995-2000 is substantial [8], occurring at rates that rival those of the entire Antarctic continent. Estimates are also available for glaciers of the Southern Alps of New Zealand [9].

The greatest uncertainty in computing southern hemispheric long wavelength gravity changes due to continental cryospheric imbalance is a lack of sound observational constraint on the Antarctic Peninsula region.

2.3 Space and Terrestrial Fields from Cryospheric Imbalances

It is straightforward to convert volumetric ice imbalance into gravity and crustal motion for elastic Earth models. First, we note that a set of surface density rate coefficients, $\dot{\bar{\sigma}}_{\ell mj}$, may be calculated in an expansion similar to (1) and related to the Stokes rate coefficients as:

$$\dot{\bar{\sigma}}_{\ell mj} \quad = \quad \frac{M}{2\pi R_e^2}(\ell + \frac{1}{2})\,\dot{\bar{C}}_{\ell mj}\ . \tag{2}$$

With the direct loading of the ocean (of total rise rate $\dot{\xi}$) accounted for, these coefficients are computed from a series of spherical caps with rates of ice height changes $\dot{D}_i$. Assuming conservation of mass, the density coefficients are

$$\dot{\bar{\sigma}}_{\ell mj} \quad = \quad \rho_{\rm ice} \sum_{i=1}^{\mathcal{I}_{\rm disk}} \tilde{w}_{\ell mj,i}\dot{D}_i \ - \ \frac{\rho_{\rm w}}{2\ell+1}\,\dot{\xi}\bar{a}_{\ell mj} \tag{3}$$

where $\rho_{\rm w}$ and $\rho_{\rm ice}$ are densities of ocean water and continental ice, and $\bar{a}_{\ell mj}$ are normed ocean coefficients [4]. The total number of caps is $\mathcal{I}_{\rm disk}$ and $\tilde{w}_{\ell mj,i}$ are disk coefficients (eq. 30b in [10]). The rate of change in the geoid [4] is:

$$\frac{d\mathsf{N}}{dt} \quad = \quad R_e \sum_{\ell=2}^{L}\sum_{m=0}^{\ell}\sum_{j=1}^{2} \dot{\bar{C}}_{\ell mj}(t)\,(1+k'_\ell)\,\bar{Y}_{\ell mj}(\theta,\lambda) \tag{4}$$

and the time-rate of change in surface gravity [10] is

$$\frac{d\delta \mathrm{g}}{dt} \quad = \quad -g \sum_{\ell=2}^{L}\sum_{m=0}^{\ell}\sum_{j=1}^{2} [\,\frac{1}{2} + (\ell+1)k'_\ell + 2h'_\ell\,]\dot{\bar{C}}_{\ell mj}(t)\,\bar{Y}_{\ell mj}(\theta,\lambda) \tag{5}$$

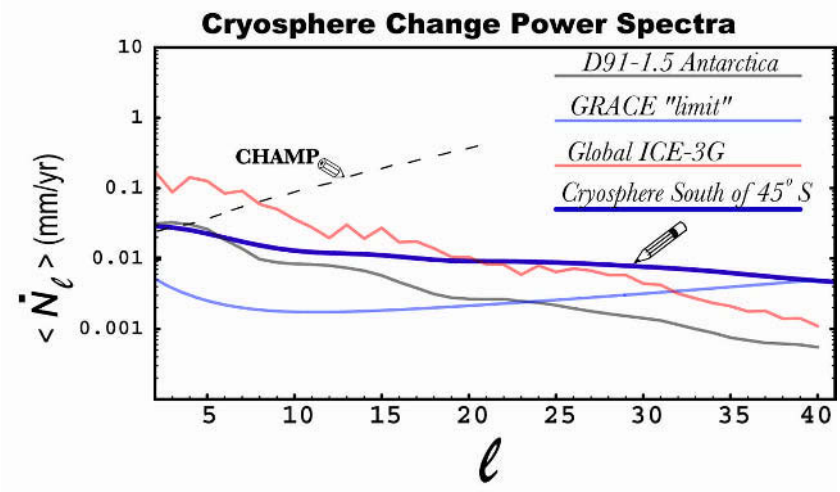

Fig. 1. Power spectra for cryosphere change and GIA models. GRACE annual recovery error estimate [1] and CHAMP sensitivity estimate for three years [14] correspond to theoretical limits.

wherein elastic deformation is accounted for by the surface potential and radial displacement Love numbers, k'_ℓ and h'_ℓ, respectively. Geoid rates may be constructed using the stand-alone satellite data. The surface rate of change is measured using absolute gravity instruments placed on bedrock [11] [12].

Integration of Present-day Cryospheric Information Using the cap-grid structure for ice covered regions, each of the terms $\tilde{w}_{\ell mj,i}\dot{D}_i$ in (3) is created with grid-size varying from small sizes in the Cordillera Darwin (Tierra del Fuego), Patagonia and the Antarctic Peninsula (radii $\alpha_i \simeq 0.05°$) to large caps in East Antarctica (radii $\alpha_i \simeq 1.28°$). Each of these were treated, in essence, as cap harmonics. For our purposes, neither spatial nor spectral smoothing was required and the series were truncated at $L = 256$, as were the ocean function coefficients. The total ESLRR associated with land-ocean mass transfer for four regions south of 42.5° S is given in Table 1. The total rate of change in sealevel, $\dot{\xi}$, in (3) is assumed to be derived from the net sum of ice mass changes in the model.

Degree Power Spectra The detectability of the time-dependent field generated by changes in the continental cryosphere may be scrutinized via the secular geoid rate power spectrum [13]. Such plots (Figure 1) are diagnostic of the ability for satellite data to recover the time-dependent field associated with the large-scale ice mass changes. In Figure 1 the combined mass exchange of all four regions (*A*, *AP*, *SSA* and New Zealand; *NZ*) are assumed. For comparison, the spectra for both global and Antarctic GIA are

also shown (see [13]). With the exception of Antarctica, GIA has a fairly reliable time-dependent gravity field.

Antarctic Peninsula Scenario The status of glacial and ice sheet balance has been greatly improved during the last few years in all but one region: the Antarctic Peninsula. Data-based models of glacier discharge that scale seasonal temperature changes to elevation and precipitation, suggest that the Peninsula is in negative mass balance [15] [16] [17]. The evidence, however, is somewhat anecdotal. (For example, the observed changes in adjacent ice shelves [18]). There is not enough data for constructing a complete balance estimate, and even the net surface mass balance is complicated by short wavelength orography [19]. We incorporate a scaled model [16] to account for the Peninsula.

While model inputs for Patagonia are likely significant at a $2-\sigma$ level [8], uncertainty of the Antarctic continent struggles at the $1-\sigma$ level [7], a situation possibly exacerbated by sub-decadal variability [20]. The estimate also considers reanalysis with newly acquired airborne laser altimetry and radio echo sounding data [21]. In spite of its large uncertainty, the new estimate is a great improvement over the simple 'scenarios' assumed previously [5] [10].

3 Terrestrial and Space Rate Predictions

3.1 Zonal Field

Observations of the amplitudes of the secular zonal harmonic rates are roughly $\mid \dot{J}_\ell \mid \sim 0.3 \longleftrightarrow 3.0 \times 10^{-11}\mathrm{yr}^{-1}$ for $2 \leq \ell \leq 6$ [6]. Table 2 gives ice change predictions for the very low order zonal gravity field rate coefficients. Clearly, these predictions are of an amplitude comparable to those derived from long-term SLR observations. For the first time, then, it is more definitively show that interdecadal cryospheric change in the high latitude Southern Hemisphere is a major contributor to the overall $\dot{J}_\ell$-sealevel budget. This is true, even if the 'AP' scenario is ignored (the column $\dot{J}_\ell^{-AP}$ in Table 2 is for coefficients computed with the net imbalance of the Peninsula set to zero).

3.2 Non-zonal and Surface Gravity Change

The non-zonal coefficient amplitude is strong enough that CHAMP, GRACE and follow-on gravity missions could be employed to 'monitor' the cryospheric balance state in the Southern Hemisphere. For such analyses, we provide the lowest 12 degree/order normed rate coefficients in Table 3 for the forward model that includes the 'AP' scenario and provide a map of the corresponding surface gravity rate change, $d\delta\mathrm{g}/dt$ in Figure 2. Measurement of the surface

Table 2. Zonal rate coefficients $\dot{J}_\ell \equiv -\sqrt{2\ell+1}\dot{\bar{C}}_{\ell 0}$ (units: $10^{-11}\mathrm{yr}^{-1}$)

ℓ	$\dot{J}_\ell$	$\dot{J}_\ell^{-AP}$	ℓ	$\dot{J}_\ell$	$\dot{J}_\ell^{-AP}$
1	-2.034	-1.587	7	-0.170	-0.218
2	1.211	0.929	8	0.055	0.163
3	-1.040	-0.780	9	0.081	-0.064
4	0.755	0.559	10	-0.266	0.104
5	-0.495	-0.381	11	0.478	0.321
6	0.298	0.270	12	-0.677	-0.542

gravity change may be important for separation of solid Earth GIA signatures from current ice mass change related gravity [22] [10]. The future for terrestrial gravity measurements may, indeed, be a bright one, due to recent technological advances that allow such instruments greater portability and lower power levels for continuous operation [23]. The predicted rates of gravity change in West Antarctica and Patagonia exceed annual change amplitude of 1.5 μgals over wavelengths of several hundred km.

3.3 Geoid Change

Continued improvements in the processing of CHAMP and GRACE data may soon mean that secular changes in the geoid shall be determined at, or below, the 1 mm level at half wavelengths, $\Delta\lambda \simeq \pi R_e/\ell$, of $\Delta\lambda \sim 1600$ km ($\ell \sim 12$) [24]. Figure 3 shows in mapview the computed annual geoid changes anticipated for cryospheric land/ocean mass transfer south of 42.5° using recent mass balance estimates [7] [8] [21]. Although preliminary analysis of CHAMP and GRACE data do not yet show this level of sensitivity, the large signal ($\sim$ -1 mm/yr) contoured over West Antarctica has $600 \leq \Delta\lambda \leq 2000$ km, and thus, there is potential for this signal to be detected.

4 Conclusions

The goal of the present paper is to clarify the current status of forward modeling predictions for interdecadal to multidecadal time-scale cryospheric change south of 42.5° S at high spatial resolution and to offer predictive maps for estimating both space and terrestrial-based gravity changes. Largely due to the application of space and airborne monitoring systems and the emergence of InSAR and GPS, great strides have been made in determining ice mass balance since about 1990. Folding such information into the various forward/inverse architectures for solving for global water mass fluxes is important in two distinct areas of gravity research: (1) analysis of mass flux budgets from the zonal field monitoring provided by SLR; and (2) for the future analyses of ice mass budgets in which high resolution data may be able

to provide an additional tool for deciphering the GIA component of secular Antarctic gravity change.

Table 3. Non-zonal rate coefficients for ice mass south of 42.5° (units: $10^{-11}\mathrm{yr}^{-1}$)

ℓ	m	$\dot{C}_{\ell m}$	$\dot{S}_{\ell m}$	ℓ	m	$\dot{C}_{\ell m}$	$\dot{S}_{\ell m}$
1	1	-0.08773	0.50261	9	4	0.01458	0.05543
2	1	0.02346	-0.43268	9	5	-0.07292	-0.00113
2	2	0.08552	0.03383	9	6	0.01382	-0.05086
3	1	-0.01104	0.48439	9	7	0.02130	0.01109
3	2	-0.14452	-0.05936	9	8	-0.00569	0.00524
3	3	0.03178	-0.03324	9	9	-0.00065	-0.00137
4	1	-0.01045	-0.46513	10	1	-0.04409	-0.19464
4	2	0.19257	0.05242	10	2	0.14171	-0.10706
4	3	-0.06405	0.05614	10	3	0.05232	0.02614
4	4	-0.00828	-0.02516	10	4	-0.00072	-0.02467
5	1	0.03937	0.40150	10	5	0.06542	0.00484
5	2	-0.19575	-0.02886	10	6	-0.01848	0.06052
5	3	0.07950	-0.07598	10	7	-0.03325	-0.01775
5	4	0.01583	0.04669	10	8	0.01150	-0.01090
5	5	-0.01305	-0.00067	10	9	0.00222	0.00465
6	1	-0.06038	-0.33111	10	10	-0.00106	0.00031
6	2	0.18137	-0.00915	11	1	0.02961	0.15748
6	3	-0.07874	0.08100	11	2	-0.15805	0.09909
6	4	-0.02673	-0.06773	11	3	-0.07236	-0.02612
6	5	0.03113	-0.00083	11	4	-0.01162	-0.00789
6	6	-0.00193	0.00743	11	5	-0.04577	-0.00992
7	1	0.07038	0.27696	11	6	0.02180	-0.06062
7	2	-0.15689	0.05078	11	7	0.04319	0.02398
7	3	0.05696	-0.07326	11	8	-0.01948	0.01825
7	4	0.02943	0.07988	11	9	-0.00525	-0.01015
7	5	-0.05086	0.00189	11	10	0.00302	-0.00091
7	6	0.00488	-0.01935	11	11	-0.00006	0.00059
7	7	0.00414	0.00241	12	1	-0.01830	-0.10427
8	1	-0.06880	-0.24268	12	2	0.17152	-0.08579
8	2	0.13730	-0.08460	12	3	0.07896	0.03729
8	3	-0.02101	0.05541	12	4	0.01921	0.03356
8	4	-0.02493	-0.07597	12	5	0.01933	0.01545
8	5	0.06719	-0.00099	12	6	-0.02387	0.04968
8	6	-0.00916	0.03514	12	7	-0.04760	-0.02821
8	7	-0.01151	-0.00576	12	8	0.02790	-0.02559
8	8	0.00206	-0.00153	12	9	0.00924	0.01796
9	1	0.05850	0.21989	12	10	-0.00731	0.00189
9	2	-0.13236	0.10379	12	11	0.00015	-0.00203
9	3	-0.01913	-0.03720	12	12	0.00045	0.00024

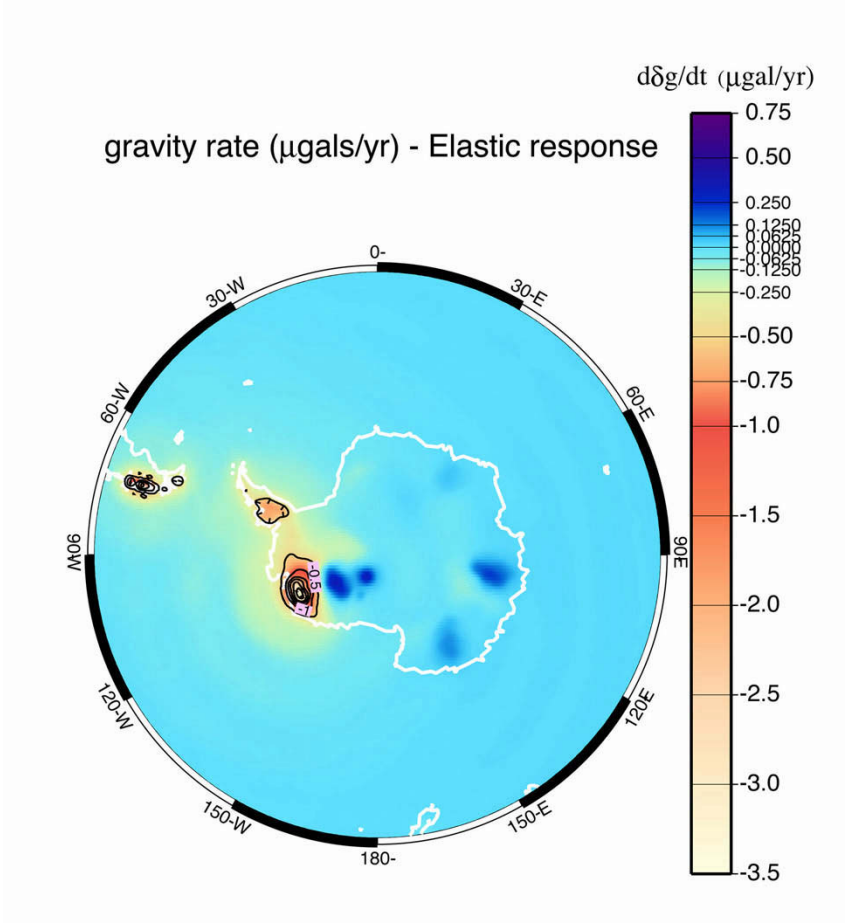

Fig. 2. Surface gravity change for absolute and relative terrestrial gravity measurements. Contours of negative $d\delta g/dt$ are at 0.5 μgal/yr intervals.

References

1. Wahr J, Molenaar M, Bryan F (1998) Time-variability of the Earth's gravity field: hydrological and oceanic effects and their possible detection using GRACE. J Geophys Res *103*: 30,231–30,229.
2. Jacobs SS, Giulivi CF, Mele PA (2002) Freshening of the Ross Sea during the late 20th Century. Science *297*: 386–389.
3. Reigber C, Balmino G, Schwintzer P, Biancale R, Bode A, Lemoine JM, Konig R, Loyer S, Neumayer H, Marty JC, Barthelmes F, Perosanz F, Zhu SY (2003) Global gravity field recovery using solely GPS tracking and accelerometer data from CHAMP. Space Sci Rev *108*: 55–66.
4. Lambeck K (1980) The Earth's Variable Rotation: Geophysical Causes and Consequences. Cambridge U. Press, Cambridge New York Sydney, pp. 449.

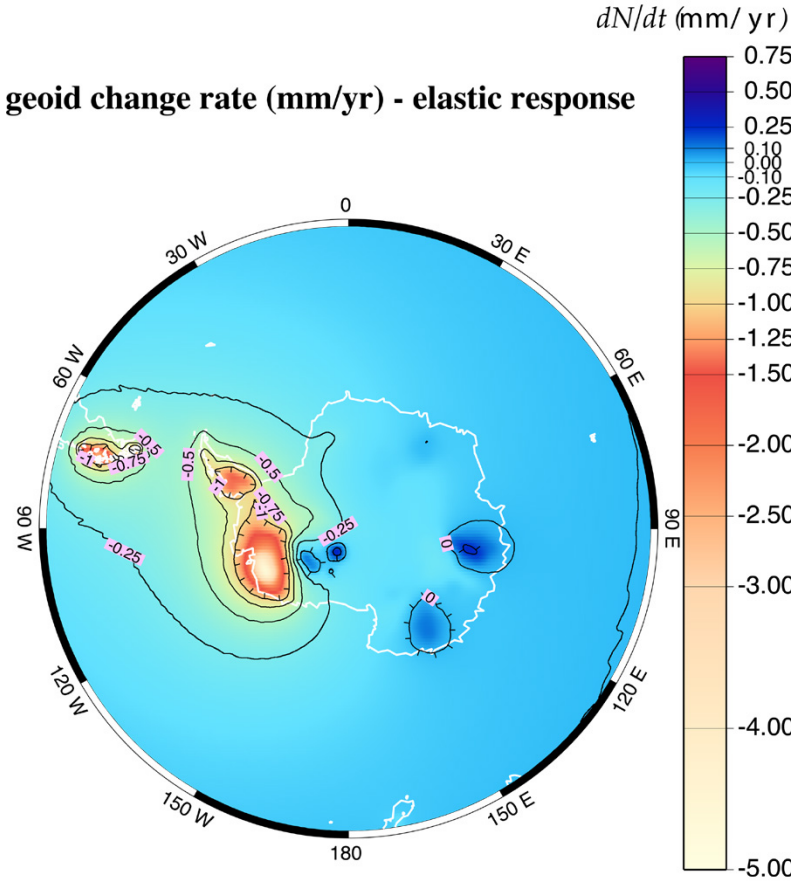

Fig. 3. Geoid changes caused by glacial imbalances, associated ocean filling and elastic response.

5. James TS, Ivins ER (1997) Global geodetic signatures of the Antarctic ice sheet. J Geophys Res *102*: 605–633.
6. Cox CM, SM Klosko BF Chao (2001) Changes in ice-mass balance inferred from time variations of the geopotental observed through SLR and DORIS tracking. In: Sideris M (ed) Gravity, geoid and geodynamics 2000: IAG symposium series *123*, Springer, Berlin Heidelberg New York: 353–360.
7. Rignot E, Thomas RH (2002) Mass balance of polar ice sheets. Science *297*: 1502–1506.
8. Rignot E, Rivera A, Casassa G (2003) Contribution of the Patagonia icefields of South America to sealevel rise. Science *302*: 434–437.
9. Dyurgerov MB, Meier MF (1997) Mass balance of mountain and subpolar glaciers: a new global assessment for 1961-1990. Arctic Alp Res *29*: 379–391.

10. James TS, Ivins ER (1998) Predictions of Antarctic crustal motions driven by present-day ice sheet evolution and by isostatic memory of the Last Glacial Maximum. J Geophys Res *103*: 4993–5017.
11. Lambert A, Laird JO, Courtier N, Bower DR (1994) Absolute gravimetry applied to postglacial rebound studies: progress in Laurentia. In: Schutz BE, Anderson A, Froidevaux C, Parke M (ed) Gravimetry and Space Techniques Applied to Geodynamics and Ocean Dynamics, Geophysical Monograph *82*, IUGG vol 17, AGU, Washington DC 1–7.
12. Amalvict M, Hinderer J, Luck B (2001) First absolute gravity measurements at the French station Dumont d'Urville (Antarctica). In: Sideras M (ed), Gravity, geoid and geodynamics 2000: IAG symposia series *123*, Springer, Berlin Heidelberg New York: 373-377.
13. Ivins ER, Wu X, Raymond CA, Yoder CF, James TS (2001) Temporal geoid of a rebounding Antarctica and potential measurement by the GRACE and GOCE satellites. In: Sideris M (ed) Gravity, geoid and geodynamics 2000: IAG symposium series *123*, Springer, Berlin Heidelberg New York: 361–366.
14. Visser PNAM, Rummel R, Balmino G, Sünkel H, Johanessen J, Aguirre M, Woodworth PL, Le Provost C, Tischering CC, Sabadini R (2002) The European Earth Explorer Mission: GOCE: Impact for the geosciences. In: Mitrovica JX, Vermerrsen B (ed) Ice Sheets, Sea Level and the Dynamics Earth, Geodynamics Series *29*, AGU Washington DC: 95–107.
15. Fox AJ, Cooper APR (1998) Climate-change indicators from archival aerial photography of the Antarctic Peninsula. Ann Glaciology *27*: 636–642.
16. Ivins ER Raymond CA, James TS (2000) The influence of 5000 year-old and younger glacial variability on present-day rebound in the Antarctic Peninsula. Earth Planets Space *52*: 1023–1029.
17. Rau F, Braun M (2002) The regional distribution of the dry-snow zone on the Antarctic Peninsula north of 70 degrees S Ann Glaciology *34*: 95-100.
18. Shepherd A, Wingham D, Payne T, Skvarca P (2003) Larsen Ice Shelf has progressively thinned. Science *302*: 856–859.
19. Turner J, Lachlan-Cope TA, Marshall GJ, Morris EM, Mulvaney R, Winter W (2002) Spatial variability of Antarctic Peninsula net surface mass balance. J Geophys Res *107(D13)*: 4173, doi:10.1029/2001JD000755.
20. Joughin I, Rignot E, Rosanova CE, Lucchitta BK, Bohlander J (2003) Timing of recent accelerations of Pine Island Glacier. Antarctic Geophys Res Lett *30*: art. no. 1706.
21. Rignot E, Thomas RH, Kanagaratnam P, Casassa G, Frederick E, Gogineni S, Krabill W, Rivera A, Russell R, Sonntag J, Swift R, Yungel J (2004) Improved estimation of the mass balance of glaciers draining into the Amundsen Sea sector of West Antarctica from the CECS/NASA 2002 Campaign. Ann Glaciology *39*, (in press).
22. Wahr J, Han D, Trupin A (1995) Predictions of vertical uplift caused by changing polar ice volumes on a viscoelastic Earth. Geophys Res Lett *22*: 977–901.
23. Vitouchkine AL, Faller JE (2002) Measurement results with a small cam-driven absolute gravimeter. Metrologia *39*: 465–469.
24. Schrama EJO (2003) Error characteristics estimated from CHAMP, GRACE and GOCE derived geoids and from satellite altimetry derived mean dynamic topography. Space Sci Rev *108*: 179–193.

Springer

http://www.springer.com/978-3-540-22804-2

Earth Observation with CHAMP
Results from Three Years in Orbit
Reigber, C.; Lühr, H.; Schwintzer, P.; Wickert, J. (Eds.)
2005, XVI, 628 p., Hardcover
ISBN: 978-3-540-22804-2